

Correspondence

1 Generalized-Spatial-Modulation-Based 2 Reduced-RF-Chain Millimeter-Wave Communications

3 Naoki Ishikawa, *Student Member, IEEE*, Rakshith Rajashekar,
4 *Member, IEEE*, Shinya Sugiura, *Senior Member, IEEE*, and
5 Lajos Hanzo, *Fellow, IEEE*

6 **Abstract**—A generalized spatial modulation (GSM)-based millimeter-
7 wave communications system is proposed. The GSM transmitter is char-
8 acterized by a lower number of radio frequency (RF) chains than the
9 number of transmit antennas; hence, it is capable of reducing both the
10 transmitter cost and the energy consumption. The antenna array align-
11 ment is optimized so as to maximize the rank of the channel matrix
12 encountered. Furthermore, we employ an array of analog beamformers,
13 which allows us to benefit both from the beamforming gain and from the
14 GSM scheme's high rate. It is demonstrated that the constrained capacity
15 of the GSM transmitter equipped with as few as two RF chains is capable
16 of approaching the performance of the full-RF spatial multiplexing having
17 eight RF chains.

18 **Index Terms**—Analog beamforming, channel capacity, constrained
19 capacity, generalized spatial modulation (GSM), line-of-sight (LoS),
20 millimeter-wave (mmWave), multiple-input multiple-output (MIMO),
21 multiplexing.

22 I. INTRODUCTION

23 Spatial modulation (SM)-aided multiple-input multiple-output
24 (MIMO) schemes are capable of increasing the attainable data rate
25 with the aid of a single radio frequency (RF) transmitter [1]. In
26 the SM transmitter, the information bits are mapped to transmitted
27 symbols by activating a single transmit antenna (TA) element out of
28 multiple TA elements, and only a single symbol is transmitted from
29 the activated TA. This allows us to avoid the interchannel interference
30 at the receiver; hence, low-complexity single-stream decoding [2], [3]
31 is applicable. Furthermore, the single-RF transmitter structure specific
32 to the SM scheme reduces static power consumption [4]. In [5] and [6],
33 the SM scheme was extended to a more flexible framework referred to
34 as the generalized SM (GSM), where multiple antenna elements are
35 simultaneously activated in each symbol duration. More specifically,
36 the GSM scheme subsumes several classic MIMO schemes, such as the
37 SM and Bell Laboratories Layered Space-Time (BLAST) schemes [7].
38 In millimeter-wave (mmWave) communications [8], the rank of the
39 MIMO channel matrix tends to be low, due to the presence of a strong

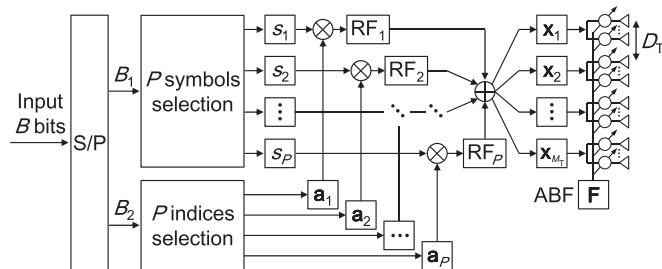


Fig. 1. Transmitter structure of our GSM scheme using an ABF array.

line-of-sight (LoS) component. In [9], the antenna alignment was
specifically adjusted for increasing the rank of the channel matrix in an 41
mmWave MIMO scenario. In [10] and [11], an antenna array architec- 42
ture of multiple beamformers was employed, where each beamformer 43
is spaced sufficiently apart from each other to experience independent 44
fading. In [12], the antenna alignment scheme [9] was applied to a 45
space-shift-keying-based mmWave system. 46

The detrimental effects of the high propagation loss in mmWave 47
communications are particularly severe in an urban scenario [8]. To 48
combat this limitation, it is beneficial to invoke beamforming at the 49
transmitter and/or the receiver [10], [11], which operates with the aid 50
of a high number of antenna elements. However, it may be disadvanta- 51
geous to employ a full-digital beamforming-array architecture that has 52
the same number of RF chains as that of the antenna elements, due to 53
their high cost and high energy consumption. Recently, a hybrid beam- 54
forming arrangement, relying on both analog and digital beamformers, 55
has been proposed in [13] and [14]. Here, a high number of antenna 56
elements are divided into beamforming subarrays, where each beam- 57
former is connected to an RF chain. Note that in the classic spatial- 58
multiplexing MIMO system, the number of RF chains has to be equal 59
to the number of multiplexed substreams. 60

Against this backdrop, the novel contribution of this letter is that 61
we provide the design guideline for the reduced-RF-chain GSM-based 62
mmWave architecture. More specifically, to benefit from both a beam- 63
forming gain and the GSM scheme's high rate, we employ an array of 64
analog beamformers (ABFs), each consisting of multiple TA elements 65
weighted by analog phase shifters. Furthermore, we optimized the 66
spacing between the ABFs, so that the rank of the associated channel 67
matrix is maximized. We demonstrate that the proposed GSM scheme 68
using the beamformer array is capable of reducing the number of RF 69
chains at the transmitter, while maintaining high capacity, which is 70
close to that of the conventional spatial-multiplexing scheme.¹ 71

72 II. SYSTEM MODEL

73 A. Reduced-RF GSM Transmitter

Fig. 1 shows the schematic of our GSM transmitter, having N_T TA 74
elements, which are partitioned into M_T ABFs, each consisting of 75
 $U_T = N_T/M_T$ TA elements and the same number of analog phase 76

¹Note that in mmWave communications, the bandwidth expansion caused by
the SM-specific antenna switching [15] may not be a major problem, because a
wide bandwidth is available.

Manuscript received December 18, 2015; revised March 10, 2016; accepted
April 14, 2016. The work of N. Ishikawa was supported in part by the SCAT
Fellowship and in part by the MEXT/JASSO Tobitate Fellowship of Japan. The
work of S. Sugiura was supported by the Japan Society for the Promotion
of Science KAKENHI under Grant 26709028. The work of L. Hanzo was
supported by the European Research Council's Advanced Fellow Grant Beam-
Me-Up. The review of this paper was coordinated by Prof. Y. L. Guan.

N. Ishikawa and S. Sugiura are with the Department of Computer and
Information Sciences, Tokyo University of Agriculture and Technology, Tokyo
184-8588, Japan (e-mail: naoki@ishikawa.cc; sugiura@ieee.org).

R. Rajashekar and L. Hanzo are with the School of Electronics and Computer
Science, University of Southampton, Southampton SO17 1BJ, U.K. (e-mail:
R.Mysore-Rajashekar@soton.ac.uk; lh@ecs.soton.ac.uk).

Color versions of one or more of the figures in this paper are available online
at <http://ieeexplore.ieee.org>.

Digital Object Identifier 10.1109/TVT.2016.2555378

TABLE I
EXAMPLE OF THE GSM SYMBOLS FOR $(M_T, P) = (4, 2)$ AND $(8, 2)$

M_T	P	$\sqrt{P}\mathbf{x}$
4	2	$\begin{bmatrix} s_1 & s_2 & 0 & 0 \\ 0 & s_1 & 0 & s_2 \end{bmatrix}^T, \begin{bmatrix} s_1 & 0 & s_2 & 0 \\ 0 & 0 & s_1 & s_2 \end{bmatrix}^T,$
8	2	$\begin{bmatrix} s_1 & 0 & 0 & s_2 & 0 & 0 & 0 & 0 \\ s_1 & 0 & 0 & 0 & s_2 & 0 & 0 & 0 \\ s_1 & 0 & 0 & 0 & 0 & s_2 & 0 & 0 \\ s_1 & 0 & 0 & 0 & 0 & 0 & s_2 & 0 \\ 0 & s_1 & s_2 & 0 & 0 & 0 & 0 & 0 \\ 0 & s_1 & 0 & s_2 & 0 & 0 & 0 & 0 \\ 0 & s_1 & 0 & 0 & s_2 & 0 & 0 & 0 \\ 0 & s_1 & 0 & 0 & 0 & s_2 & 0 & 0 \end{bmatrix}^T, \begin{bmatrix} 0 & 0 & s_1 & s_2 & 0 & 0 & 0 & 0 \\ 0 & 0 & s_1 & 0 & 0 & s_2 & 0 & 0 \\ 0 & 0 & s_1 & 0 & 0 & 0 & s_2 & 0 \\ 0 & 0 & 0 & s_1 & 0 & s_2 & 0 & 0 \\ 0 & 0 & 0 & 0 & s_1 & 0 & s_2 & 0 \\ 0 & 0 & 0 & 0 & 0 & s_1 & 0 & s_2 \\ 0 & 0 & 0 & 0 & 0 & 0 & s_1 & 0 \\ 0 & 0 & 0 & 0 & 0 & 0 & 0 & s_1 \end{bmatrix}^T,$

77 shifters. In our GSM transmitter, the number of RF chains P is less 78 than the number of ABFs M_T , whereas the conventional spatial- 79 multiplexing scheme requires a full-RF structure having $P = M_T$.

80 At the GSM transmitter, B information bits are mapped into 81 a symbol vector $\mathbf{x} \in \mathbb{C}^{M_T \times 1}$ as follows. The B input bits are 82 serial-to-parallel converted into $B_1 = P \log_2(\mathcal{L})$ bits and $B_2 =$ 83 $\lceil \log_2 \binom{M_T}{P} \rceil$ bits. The B_1 bits are modulated to P complex-valued 84 symbols s_p ($p = 1, \dots, P$) with the aid of the classic quadrature 85 amplitude modulation (QAM) or phase-shift keying (PSK) scheme, 86 where the constellation size is given by \mathcal{L} . Based on the B_2 bits, 87 P out of M_T ABFs are activated, where P index vectors $\mathbf{a}_p \in$ 88 $\mathbb{C}^{M_T \times 1}$ ($p = 1, \dots, P$) are selected out of the M_T legitimate vectors 89 of $([1 \ 0 \ \dots \ 0]^T, [0 \ 1 \ \dots \ 0]^T, \dots, [0 \ 0 \ \dots \ 1]^T)$. Finally, the GSM 90 transmitter generates a symbol vector \mathbf{x} according to

$$\mathbf{x} = \frac{1}{\sqrt{P}} \sum_{p=1}^P s_p \mathbf{a}_p \quad (1)$$

91 which satisfies the average power constraint of $E[\|\mathbf{x}\|^2] = 1$, where 92 $E[\bullet]$ represents the expectation operation. In advance of trans- 93 missions, the symbol vector \mathbf{x} is precoded by a matrix $\mathbf{F} =$ 94 $\text{diag}(\mathbf{f}_1, \dots, \mathbf{f}_{M_T}) \in \mathbb{C}^{N_T \times M_T}$ [10], [11], where $\text{diag}(\bullet)$ represents 95 the block diagonalization, and $\mathbf{f}_i \in \mathbb{C}^{U_T \times 1}$ ($1 \leq i \leq M_T$) represents 96 the weight vectors of the i th ABF at the transmitter, which has the 97 constraint of $\|\mathbf{f}_i\|^2 = 1$.

98 To further elaborate, in Table I, we exemplify the GSM symbol sets 99 for the $(M_T, P) = (4, 2)$ and $(8, 2)$ scenarios. Furthermore, note that 100 the classic spatial multiplexing is a special case of the GSM scheme, 101 where the number of RF chains P is equal to the number of ABFs 102 M_T . Similarly, the conventional single-stream symbol transmission is 103 also subsumed by the GSM framework, where we have $P = 1$ and 104 $\mathbf{a}_1 = [1 \ 1 \ \dots \ 1]^T / \sqrt{M_T}$.

105 B. Channel Model

106 In this paper, we focus our attention on indoor mmWave commu- 107 nications, where a LoS component has the dominant effect [10]–[12], 108 [16], [17] in comparison to the non-LoS paths. More specifically, we 109 employ the frequency-flat Rician channel model. Fig. 2 shows the 110 alignment of the ABF-array transmitter and receiver. The spacing be- 111 tween the ABF arrays at the transmitter and the receiver is represented 112 by D_T and D_R , respectively. Moreover, d is the element separation of 113 each antenna element. The transmitter is located at a height of R . The 114 receiver has N_R antennas, and it is tilted at an angle of θ .

115 The Rician fading channels are given by [9], [10], [12]

$$\mathbf{H} = \sqrt{\frac{K}{K+1}} \mathbf{H}_{\text{LoS}} + \sqrt{\frac{1}{K+1}} \mathbf{H}_{\text{NLoS}} \in \mathbb{C}^{N_R \times N_T} \quad (2)$$

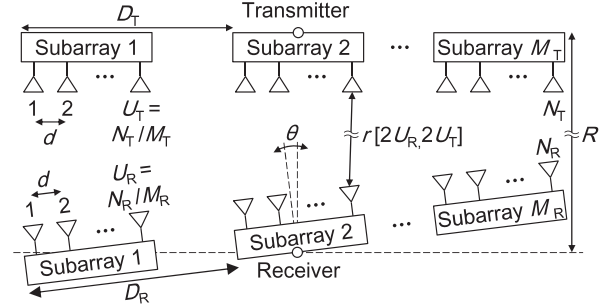


Fig. 2. ABF-array arrangement of our GSM transmitter and receiver. The transmitter is located at a height of R , and the receiver is tilted at an angle of θ .

where K is the Rice factor. Note that for the 60-GHz indoor communi- 116 cations scenario, the Rice factor K is in the range spanning from 8.34 117 to 12.04 dB [16]. Here, let us define the n th row and the m th column of 118 \mathbf{H}_{LoS} by $\mathbf{H}_{\text{LoS}}[n, m] = \exp(-j \cdot (2\pi/\lambda) \cdot r[n, m])$, where $r[n, m]$ 119 is the distance between the m th TA and the n th receive antenna, 120 whereas λ represents the wavelength. Furthermore, the n th row and the 121 m th column of \mathbf{H}_{NLoS} obeys the zero-mean complex-valued Gaussian 122 distribution, having a unit variance. 123

C. Receiver

124 Similar to the transmitter, the receiver consists of M_R ABFs, each 125 having $U_R = N_R/M_R$ antenna elements. The receiver is equipped 126 with the same number of RF chains as that of the ABFs, hence having 127 a full-RF structure of $P = M_R$. The signals received at the M_R ABFs 128 are given by 129

$$\mathbf{y} = \underbrace{\mathbf{W}^H \mathbf{H} \mathbf{F}}_{\mathbf{H}_b} \mathbf{x} + \mathbf{n} \in \mathbb{C}^{M_R} \quad (3)$$

where $\mathbf{W} = \text{diag}(\mathbf{w}_1, \dots, \mathbf{w}_{M_R}) \in \mathbb{C}^{N_R \times M_R}$ [10], [11] is the ABF 130 weight matrix associated with the analog phase shifters at the re- 131 ceiver, which satisfies the constraint of $\|\mathbf{w}_k\|^2 = 1$ ($1 \leq k \leq M_R$). 132 Furthermore, $\mathbf{n} \in \mathbb{C}^{M_R \times 1}$ denotes the additive white Gaussian noise 133 having the variance of N_0 , whereas $\mathbf{W}^H \mathbf{H} \mathbf{F}$ is represented by the 134 equivalent channel matrix $\mathbf{H}_b \in \mathbb{C}^{M_R \times M_T}$. In this paper, we assume 135 that the receiver acquires accurate channels \mathbf{H}_b with the aid of pilot 136 symbols transmitted from the transmitter. Furthermore, the direction 137 between the transmitter and the receiver is also known, which is used 138 to determine the ABF weights \mathbf{F} and \mathbf{W} at the transmitter and the 139 receiver, as will be shown in Section III-D. 140

Finally, the receiver estimates the transmitted information bits 141 (B_1, B_2) , based on the maximum-likelihood criterion as follows: 142

$$(\hat{B}_1, \hat{B}_2) = \arg \min_{(B_1, B_2)} \|\mathbf{y} - \mathbf{H}_b \mathbf{x}\|^2. \quad (4)$$

The reduced-complexity detection algorithms [2], [3], [18] developed 143 for the GSM are readily applicable to the proposed receiver. 144

III. CHANNEL CAPACITY

145 Here, we review the continuous-input–continuous-output memo- 146 ryless channel (CCMC) capacity and the discrete-input–continuous- 147 output memoryless channel (DCMC) capacity for our mmWave GSM 148 scheme. The CCMC capacity is derived by assuming that the input 149 signal obeys the Gaussian distribution, whereas in the derivation of the 150 DCMC capacity, a specific finite-alphabet input symbol set is assumed. 151

152 A. CCMC Capacity

153 The classic CCMC capacity C_{CCMC} is given by [10], [14]

$$C_{\text{CCMC}} = E_{\mathbf{H}} \left[\sum_{i=1}^{\text{rank}(\mathbf{Q})} \log_2(1 + \mu_i \rho) \right] \text{ [bits/symbol]} \quad (5)$$

154 where we have

$$\mathbf{Q} = \begin{cases} \mathbf{H}_b^H \mathbf{H}_b & (M_R \geq M_T) \\ \mathbf{H}_b \mathbf{H}_b^H & (M_R < M_T). \end{cases} \quad (6)$$

155 Here, μ_i is the i th eigenvalue of the Hermitian matrix \mathbf{Q} , while
 156 assuming continuous-amplitude discrete-time signaling. Moreover, ρ
 157 represents the signal-to-noise ratio (SNR). In the CCMC capacity of
 158 (5), the employment of ideal ABF weights \mathbf{F} and \mathbf{W} is assumed at the
 159 transmitter and the receiver, where \mathbf{F} is the M_T right singular vectors
 160 of \mathbf{H} associated with the maximum singular values. Similarly, \mathbf{W} is
 161 the M_R left singular vectors of \mathbf{H} .

162 B. DCMC Capacity

163 Let us now introduce the DCMC capacity C_{DCMC} of mmWave
 164 MIMO systems as follows [19], [20]:

$$C_{\text{DCMC}} = B - \frac{1}{2^B} \sum_{f=1}^{2^B} E_{\mathbf{H}, \mathbf{n}} \left[\log_2 \sum_{g=1}^{2^B} e^{\eta[f, g]} \right] \text{ [bits/symbol]} \quad (7)$$

165 where we have

$$\eta[f, g] = \frac{-\|\mathbf{H}_b(\mathbf{x}_f - \mathbf{x}_g) + \mathbf{n}\|^2 + \|\mathbf{n}\|^2}{N_0} \quad (8)$$

166 and \mathbf{x}_i ($i = 1, \dots, 2^B$) represents the legitimate symbol vectors.
 167 The ABF weight matrices \mathbf{F} and \mathbf{W} are generated according to the
 168 criteria presented in Section III-D. Note that powerful channel coding
 169 schemes, such as the turbo codes or low-density parity-check codes,
 170 allow us to attain a near-error-free performance close to the DCMC
 171 capacity [21].

172 C. Optimization of ABF-Array Alignment

173 As previously mentioned, the rank of the MIMO channel matrix
 174 in an indoor mmWave scenario is typically low. To circumvent this
 175 problem, we optimize the ABF-array alignment according to [9],
 176 which increases the rank of the channel matrix. More specifically, to
 177 attain the optimum performance in terms of the rank of the channel
 178 matrix, the separations of the ABFs D_T and D_R at the transmitter and
 179 the receiver have to satisfy the following relationship [9]–[11]:

$$D_T D_R = \frac{\lambda R}{\max(M_T, M_R) \cos(\theta)} \quad (9)$$

180 where the maximum rank of the channel matrix is given by
 181 $\text{rank}(\mathbf{H}_b) = \min(M_T, M_R)$.

182 D. Criterion for Determining the ABF Weights

183 If the transmitter knows the accurate estimates of the channel \mathbf{H} ,
 184 which has as many as $(N_T \cdot N_R)$ channel coefficients, it is possible
 185 to carry out optimum beamforming at the transmitter and the receiver.
 186 However, in practice, it may be a challenging task to acquire all the
 187 $(N_T \cdot N_R)$ channel coefficients, particularly for a large-scale MIMO
 188 scenario. Hence, in this paper, we control the ABFs based only on
 189 the angle-of-departure (AoD) θ_{AoD} and the angle-of-arrival (AoA)

TABLE II
SYSTEM PARAMETERS

Fig.	Rate	Scheme	RF	\mathcal{L}	Rate	Scheme	RF	\mathcal{L}
3	4.0	BF	1	16	8.0	BF	1	256
	4.0	BLAST	2	4	8.0	BLAST	2	16
	4.0	BLAST	4	2	8.0	BLAST	4	4
	4.0	GSM	1	4	8.0	GSM	1	64
	4.0	GSM	2	2	8.0	GSM	2	8
4	8.0	BF	1	256	16.0	BF	1	65536
	8.0	BLAST	2	16	16.0	BLAST	2	256
	8.0	BLAST	8	2	16.0	BLAST	8	4
	8.0	GSM	1	32	17.0	GSM	1	16384
	8.0	GSM	2	4	16.0	GSM	2	64

θ_{AoA} at the transmitter and the receiver, respectively. This significantly
 190 reduces the number of channel coefficients that have to be estimated
 191 from the transmitted pilot symbols, namely, from $(N_T \cdot N_R)$ to $(M_T \cdot 192$
 $M_R)$, which is lower than that needed for the full-digital array. More
 193 specifically, the ABF weights \mathbf{f}_i and \mathbf{w}_k are given by [10], [13] 194

$$\mathbf{f}_i = \frac{1}{\sqrt{U_T}} \left[1, \exp(j\delta_T^{(i)}), \dots, \exp(j(U_T - 1)\delta_T^{(i)}) \right]^T$$

$$\mathbf{w}_k = \frac{1}{\sqrt{U_R}} \left[1, \exp(j\delta_R^{(k)}), \dots, \exp(j(U_R - 1)\delta_R^{(k)}) \right]^T$$

where we have $\delta_T^{(i)} = d \cdot (2\pi/\lambda) \cdot \sin(\theta_{\text{AoD}}^{(i)})$ and $\delta_R^{(k)} = d \cdot (2\pi/\lambda) \cdot 195$
 $\sin(\theta_{\text{AoA}}^{(k)})$.² Here, $\theta_{\text{AoD}}^{(i)}$ denotes the AoD toward the i th ABF of the 196
 receiver, whereas $\theta_{\text{AoA}}^{(k)}$ represents the AoA from the k th ABF of the 197
 transmitter. 198

IV. PERFORMANCE RESULTS

199

Here, we provide our performance results to characterize the ca-
 200 pacity of our GSM scheme, which is compared with the single-stream
 201 BF and the spatial-multiplexing benchmark schemes. Throughout the 202
 simulations, we assumed the indoor mmWave scenario in Fig. 2, 203
 where we have an antenna height of $R = 5$ m. We considered the 204
 carrier frequency of 60 GHz, where the corresponding wavelength was 205
 $\lambda = 0.5$ cm. The Rice factor K was set to 10.0 dB in accordance with 206
 the work in [11]. The antenna spacing d in each ABF was fixed to $\lambda/2$, 207
 and the separation between ABFs was optimized based on (9). The 208
 employment of omnidirectional antenna elements was assumed both 209
 at the transmitter and the receiver. Furthermore, system parameters of 210
 all schemes are listed in Table II. 211

Fig. 3 compares the DCMC capacity of the GSM, the spatial-
 212 multiplexing, and the single-stream BF schemes, where the data rates 213
 were 4.0 bits/symbol (top) and 8.0 bits/symbol (bottom). The transmit- 214
 ter and the receiver have $N_T = N_R = 16$ antenna elements, which are 215
 grouped into $M_T = M_R = 4$ ABFs, where the separation of ABFs 216
 was $D_T = D_R = 7.91$ cm. In this scenario, the rank of the chan- 217
 nel matrix was $\text{rank}(\mathbf{H}_b) = \min(4, 4) = 4$. For the 4.0-bits/symbol 218
 scenario, we considered the 16-QAM single-input single-output (SISO) 219
 scheme, the binary phase-shift keying (BPSK)-aided spatial multi- 220
 plexing having $P = 4$ RF chains, the quaternary phase-shift keying 221
 (QPSK)-aided single-RF GSM scheme, and the BPSK-aided GSM 222
 having $P = 2$ RF chains. Additionally, the capacity curve of the 223
 QPSK-aided spatial-multiplexing scheme using $P = 2$ RF chains 224
 was plotted. For the case of 8.0 bits/symbol, the 256-QAM SISO 225
 scheme, the QPSK-aided spatial-multiplexing scheme having $P = 4$ 226
 RF chains, the 16-QAM-aided spatial-multiplexing scheme using 227

²Potentially, the channel state information available at the transmitter allows
 us to utilize the phase-rotation-based precoding scheme in [22].

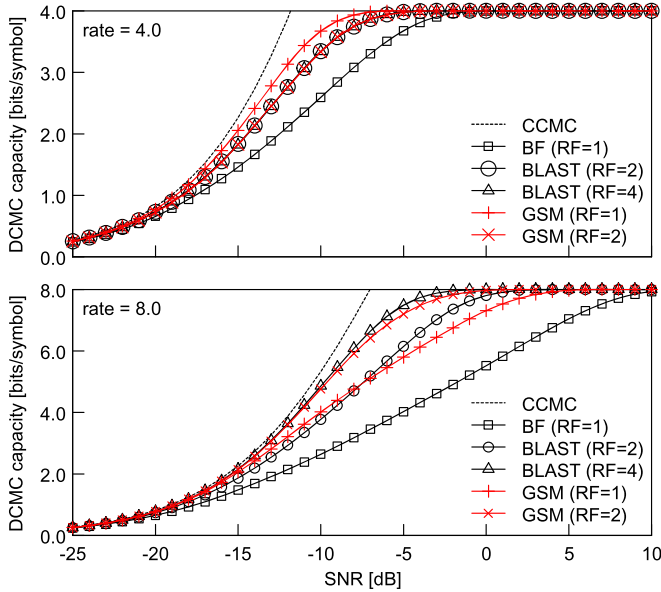


Fig. 3. DCMC capacity comparisons between the GSM and other benchmarks. The transmitter and the receiver had four ABFs, each having four antenna elements and four analog phase shifters. The associated CCMC capacity was also plotted.

228 $P = 2$ RF chains, the 64-QAM single-RF GSM scheme, and the
 229 8-PSK GSM scheme having $P = 2$ RF chains were considered. Observe
 230 in Fig. 3 that for the rate of 4.0 bits/symbol, the single-RF GSM outper-
 231 formed the other schemes. Moreover, the DCMC capacity of the GSM
 232 having $P = 2$ RF chains was close to those of the spatial-multiplexing
 233 schemes that employ $P = 2$ and 4 RF chains. Furthermore, for the rate
 234 of 8.0 bits/symbol, the DCMC capacity of the single-RF GSM scheme
 235 achieved comparable performance to that of the spatial-multiplexing
 236 scheme having $P = 2$ RF chains, whereas the DCMC capacity of the
 237 GSM scheme having $P = 2$ RF chains and the spatial-multiplexing
 238 scheme having $P = 4$ RF chains exhibited a similar performance at
 239 the transmission rate of 4.0 bits/symbol. According to our extensive
 240 simulations, it was found that the performance advantage of the
 241 proposed scheme remains unchanged in the range of $1 \leq R \leq 5$ m.

242 Moreover, Fig. 4 shows the DCMC capacity of the GSM, of the
 243 BLAST, and of the SISO schemes for the data rates of 8.0 bits/symbol
 244 (top) and 16.0 bits/symbol (bottom). The transmitter and the receiver
 245 have $N_T = 32$ and $N_R = 16$ antenna elements, respectively, where
 246 the transmitter has $M_T = 8$ ABFs, and the receiver has $M_R = 4$ ABFs.
 247 Here, the optimized separation between ABFs was $D_T = D_R =$
 248 5.59 cm. In this scenario, the rank of the channel matrix was
 249 $\text{rank}(\mathbf{H}_b) = \min(8, 4) = 4$. For the rate of 8.0 bits/symbol, the
 250 256-QAM SISO scheme, the BPSK-aided spatial-multiplexing scheme
 251 having $P = 8$ RF chains, the 16-QAM spatial-multiplexing scheme
 252 using $P = 2$ RF chains, the 32-PSK single-RF GSM scheme, and
 253 the QPSK-aided GSM using $P = 2$ RF chains were considered. For
 254 the case of 16.0 bits/symbol, the 65536-QAM SISO scheme, the
 255 QPSK-aided spatial-multiplexing scheme having $P = 8$ RF chains,
 256 the 256-QAM spatial-multiplexing scheme having $P = 2$ RF chains,
 257 the 16384-QAM single-RF GSM scheme, and the 64-QAM GSM
 258 scheme having $P = 2$ RF chains were compared. For ease of compari-
 259 son, the data rate of the single-RF GSM was set to 17.0 bits/symbol. It
 260 was shown in Fig. 4 that for the rate of 8.0 bits/symbol, the DCMC ca-
 261 pacity of the GSM scheme having two RF chains was the highest. For
 262 the rate of 16.0 bits/symbol, the full-RF spatial-multiplexing scheme
 263 exhibited the best capacity over the entire SNR region, whereas the
 264 GSM scheme having two RF chains achieved capacity close to that of

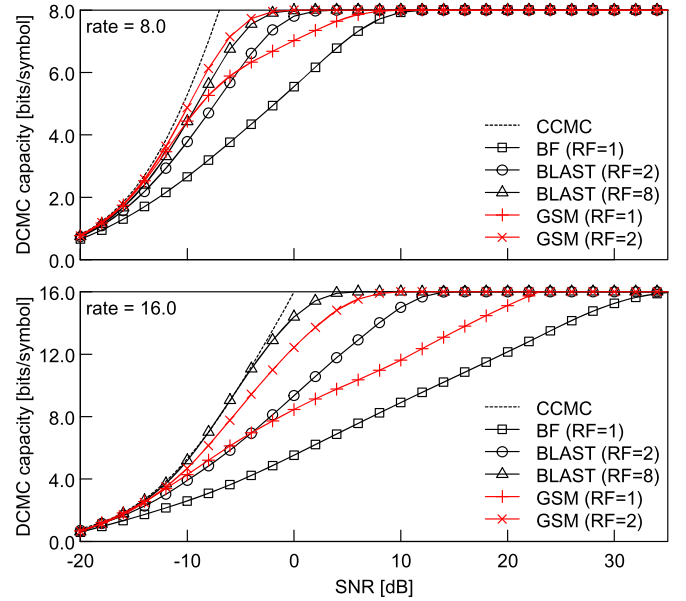


Fig. 4. DCMC capacity comparisons between the GSM and other benchmarks. The transmitter consists of eight ABFs, each having four TA elements, whereas the receiver has four ABFs, each having four receive antenna elements. The associated CCMC capacity was also plotted.

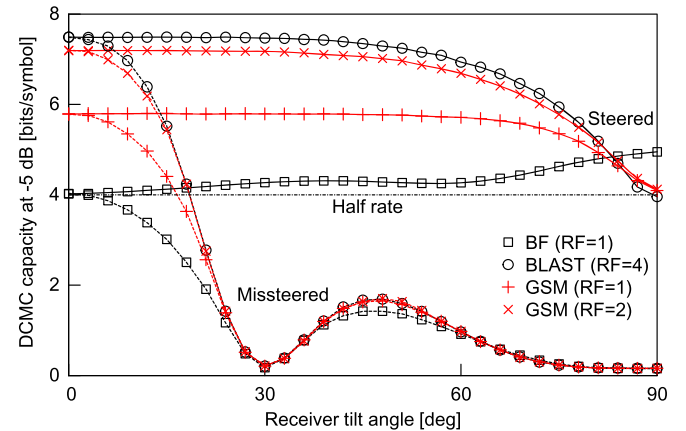


Fig. 5. Effects of the estimated tilt angle $\hat{\theta}$ on the DCMC capacity at the SNR of -5 dB. The system parameters were the same as those used in Fig. 3.

the full-RF spatial-multiplexing scheme, where the performance gap
 265 was as low as 1.2 dB for the DCMC capacity of 8.0 bits/symbol. Note
 266 that the performance advantage of the single-RF GSM scheme was
 267 approximately 9.0 dB.
 268

Finally, in Fig. 5, we investigated the effects of the receiver tilt θ ,
 269 where the system parameters were the same as those used in Fig. 3
 270 (8.0 bits/symbol). The DCMC capacity was calculated at the SNR
 271 of -5 dB. We also considered the missteered scenario, where the
 272 estimated θ_{A_oD} and θ_{A_oA} were fixed to 0° . The three capacity curves
 273 of the missteered scenario exhibited two peaks, namely, at $\theta = 0^\circ$ and
 274 45° , which corresponded to the directive gains of the main lobe and
 275 the sidelobe. When θ_{A_oD} and θ_{A_oA} were accurately estimated, the
 276 capacity of the GSM and of the spatial-multiplexing schemes remained
 277 high for the range of $0 \leq \theta < 83^\circ$.
 278

V. CONCLUSION

279

In this paper, we have proposed a GSM-based reduced-RF-chain
 280 mmWave MIMO system, where the transmitter consists of ABF arrays. 281

282 In our simulations, we demonstrated that the constrained capacity of
 283 our GSM scheme was close to that of its full-RF spatial-multiplexing
 284 counterpart, which is equipped with twice or four times higher number
 285 of RF chains than the proposed GSM scheme.

REFERENCES

- 286
 287 [1] R. Y. Mesleh, H. Haas, S. Sinanovic, C. Ahn, and S. Yun, "Spatial
 288 modulation," *IEEE Trans. Veh. Technol.*, vol. 57, no. 4, pp. 2228–2241,
 289 Jul. 2008.
- 290 [2] S. Sugiura, C. Xu, S. Ng, and L. Hanzo, "Reduced-complexity coherent
 291 versus non-coherent QAM-aided space-time shift keying," *IEEE Trans.*
 292 *Commun.*, vol. 59, no. 11, pp. 3090–3101, Nov. 2011.
- 293 [3] C. Xu, S. Sugiura, S. X. Ng, and L. Hanzo, "Spatial modulation
 294 and space-time shift keying: Optimal performance at a reduced detec-
 295 tion complexity," *IEEE Trans. Commun.*, vol. 61, no. 1, pp. 206–216,
 296 Jan. 2013.
- 297 [4] M. Di Renzo, H. Haas, A. Ghayeb, S. Sugiura, and L. Hanzo, "Spatial
 298 modulation for generalized MIMO: Challenges, opportunities, and imple-
 299 mentation," *Proc. IEEE*, vol. 102, no. 1, pp. 56–103, Jan. 2014.
- 300 [5] J. Jeganathan, A. Ghayeb, and L. Szczecinski, "Generalized space shift
 301 keying modulation for MIMO channels," in *Proc. IEEE Int. Symp.*
 302 *PIMRC*, Sep. 2008, pp. 1–5.
- 303 [6] S. Sugiura, S. Chen, and L. Hanzo, "Generalized space-time shift
 304 keying designed for flexible diversity-, multiplexing- and complexity-
 305 tradeoffs," *IEEE Trans. Wireless Commun.*, vol. 10, no. 4, pp. 1144–1153,
 306 Apr. 2011.
- 307 [7] P. Wolniansky, G. Foschini, G. Golden, and R. Valenzuela, "V-BLAST:
 308 An architecture for realizing very high data rates over the rich-scattering
 309 wireless channel," in *Proc. ISSSE*, 1998, pp. 295–300.
- 310 [8] S. Rangan, T. S. Rappaport, and E. Erkip, "Millimeter-wave cellular wire-
 311 less networks: Potentials and challenges," *Proc. IEEE*, vol. 102, no. 3,
 312 pp. 366–385, Mar. 2014.
- 313 [9] F. Bøhagen, P. Orten, and G. E. Øien, "Design of optimal high-rank line-
 314 of-sight MIMO channels," *IEEE Trans. Wireless Commun.*, vol. 6, no. 4,
 315 pp. 1420–1424, Apr. 2007.
- [10] E. Torkildson, U. Madhow, and M. Rodwell, "Indoor millimeter wave 316
 MIMO: Feasibility and performance," *IEEE Trans. Wireless Commun.*, 317
 vol. 10, no. 12, pp. 4150–4160, Dec. 2011. 318
- [11] L. Zhou and Y. Ohashi, "Fast codebook-based beamforming training for 319
 mmWave MIMO systems with subarray structures," in *Proc. IEEE 82nd* 320
Veh. Technol. Conf., 2015, pp. 1–5. 321
- [12] P. Liu and A. Springer, "Space shift keying for LOS communication 322
 at mmWave frequencies," *IEEE Wireless Commun. Lett.*, vol. 4, no. 2, 323
 pp. 121–124, Apr. 2015. 324
- [13] Y. J. Guo, X. Huang, and V. Dyadyuk, "A hybrid adaptive antenna ar- 325
 ray for long-range mm-wave communications," *IEEE Antennas Propag.* 326
Mag., vol. 54, no. 2, pp. 271–282, Apr. 2012. 327
- [14] O. E. Ayach, S. Rajagopal, S. Abu-Surra, Z. Pi, and R. W. Heath, "Spa- 328
 tially sparse precoding in millimeter wave MIMO systems," *IEEE Trans.* 329
Wireless Commun., vol. 13, no. 3, pp. 1499–1513, Mar. 2014. 330
- [15] K. Ishibashi and S. Sugiura, "Effects of antenna switching on band- 331
 limited spatial modulation," *IEEE Wireless Commun. Lett.*, vol. 3, no. 4, 332
 pp. 345–348, Aug. 2014. 333
- [16] I. Sarris and A. R. Nix, "Rician K-factor measurements in a home and 334
 an office environment in the 60 GHz band," in *Proc. 16th IST Mobile* 335
Wireless Commun. Summit, 2007, pp. 1–5. 336
- [17] Y. Shoji, H. Sawada, C. S. Choi, and H. Ogawa, "A modified SV-model 337
 suitable for line-of-sight desktop usage of millimeter-wave WPAN sys- 338
 tems," *IEEE Trans. Antennas Propag.*, vol. 57, no. 10, pp. 2940–2948, 339
 Oct. 2009. 340
- [18] R. Rajashekar, K. V. S. Hari, and L. Hanzo, "Reduced-complexity ML de- 341
 tection and capacity-optimized training for spatial modulation systems," 342
IEEE Trans. Commun., vol. 62, no. 1, pp. 112–125, Jan. 2014. 343
- [19] S. X. Ng and L. Hanzo, "On the MIMO channel capacity of multi- 344
 dimensional signal sets," *IEEE Trans. Veh. Technol.*, vol. 55, no. 2, 345
 pp. 528–536, Mar. 2006. 346
- [20] S. Sugiura, S. Chen, and L. Hanzo, "Coherent and differential space-time 347
 shift keying: A dispersion matrix approach," *IEEE Trans. Commun.*, 348
 vol. 58, no. 11, pp. 3219–3230, Nov. 2010. 349
- [21] L. Hanzo, O. Alamri, M. El-Hajjar, and N. Wu, *Near-Capacity Multi-* 350
Functional MIMO Systems. New York, NY, USA: Wiley, 2009. 351
- [22] P. Yang *et al.*, "Phase rotation-based precoding for spatial modulation 352
 systems," *IET Commun.*, vol. 9, no. 10, pp. 1315–1323, Jul. 2015. 353

AUTHOR QUERY

NO QUERY.

Correspondence

1 Generalized-Spatial-Modulation-Based 2 Reduced-RF-Chain Millimeter-Wave Communications

3 Naoki Ishikawa, *Student Member, IEEE*, Rakshith Rajashekar,
4 *Member, IEEE*, Shinya Sugiura, *Senior Member, IEEE*, and
5 Lajos Hanzo, *Fellow, IEEE*

6 **Abstract**—A generalized spatial modulation (GSM)-based millimeter-
7 wave communications system is proposed. The GSM transmitter is char-
8 acterized by a lower number of radio frequency (RF) chains than the
9 number of transmit antennas; hence, it is capable of reducing both the
10 transmitter cost and the energy consumption. The antenna array align-
11 ment is optimized so as to maximize the rank of the channel matrix
12 encountered. Furthermore, we employ an array of analog beamformers,
13 which allows us to benefit both from the beamforming gain and from the
14 GSM scheme's high rate. It is demonstrated that the constrained capacity
15 of the GSM transmitter equipped with as few as two RF chains is capable
16 of approaching the performance of the full-RF spatial multiplexing having
17 eight RF chains.

18 **Index Terms**—Analog beamforming, channel capacity, constrained
19 capacity, generalized spatial modulation (GSM), line-of-sight (LoS),
20 millimeter-wave (mmWave), multiple-input multiple-output (MIMO),
21 multiplexing.

22 I. INTRODUCTION

23 Spatial modulation (SM)-aided multiple-input multiple-output
24 (MIMO) schemes are capable of increasing the attainable data rate
25 with the aid of a single radio frequency (RF) transmitter [1]. In
26 the SM transmitter, the information bits are mapped to transmitted
27 symbols by activating a single transmit antenna (TA) element out of
28 multiple TA elements, and only a single symbol is transmitted from
29 the activated TA. This allows us to avoid the interchannel interference
30 at the receiver; hence, low-complexity single-stream decoding [2], [3]
31 is applicable. Furthermore, the single-RF transmitter structure specific
32 to the SM scheme reduces static power consumption [4]. In [5] and [6],
33 the SM scheme was extended to a more flexible framework referred to
34 as the generalized SM (GSM), where multiple antenna elements are
35 simultaneously activated in each symbol duration. More specifically,
36 the GSM scheme subsumes several classic MIMO schemes, such as the
37 SM and Bell Laboratories Layered Space-Time (BLAST) schemes [7].
38 In millimeter-wave (mmWave) communications [8], the rank of the
39 MIMO channel matrix tends to be low, due to the presence of a strong

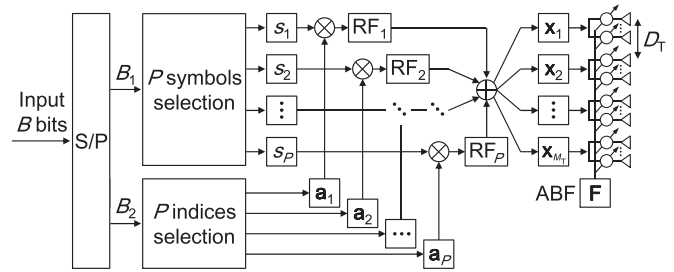


Fig. 1. Transmitter structure of our GSM scheme using an ABF array.

line-of-sight (LoS) component. In [9], the antenna alignment was 40
specifically adjusted for increasing the rank of the channel matrix in an 41
mmWave MIMO scenario. In [10] and [11], an antenna array architec- 42
ture of multiple beamformers was employed, where each beamformer 43
is spaced sufficiently apart from each other to experience independent 44
fading. In [12], the antenna alignment scheme [9] was applied to a 45
space-shift-keying-based mmWave system. 46

The detrimental effects of the high propagation loss in mmWave 47
communications are particularly severe in an urban scenario [8]. To 48
combat this limitation, it is beneficial to invoke beamforming at the 49
transmitter and/or the receiver [10], [11], which operates with the aid 50
of a high number of antenna elements. However, it may be disadvanta- 51
geous to employ a full-digital beamforming-array architecture that has 52
the same number of RF chains as that of the antenna elements, due to 53
their high cost and high energy consumption. Recently, a hybrid beam- 54
forming arrangement, relying on both analog and digital beamformers, 55
has been proposed in [13] and [14]. Here, a high number of antenna 56
elements are divided into beamforming subarrays, where each beam- 57
former is connected to an RF chain. Note that in the classic spatial- 58
multiplexing MIMO system, the number of RF chains has to be equal 59
to the number of multiplexed substreams. 60

Against this backdrop, the novel contribution of this letter is that 61
we provide the design guideline for the reduced-RF-chain GSM-based 62
mmWave architecture. More specifically, to benefit from both a beam- 63
forming gain and the GSM scheme's high rate, we employ an array of 64
analog beamformers (ABFs), each consisting of multiple TA elements 65
weighted by analog phase shifters. Furthermore, we optimized the 66
spacing between the ABFs, so that the rank of the associated channel 67
matrix is maximized. We demonstrate that the proposed GSM scheme 68
using the beamformer array is capable of reducing the number of RF 69
chains at the transmitter, while maintaining high capacity, which is 70
close to that of the conventional spatial-multiplexing scheme.¹ 71

72 II. SYSTEM MODEL

73 A. Reduced-RF GSM Transmitter

Fig. 1 shows the schematic of our GSM transmitter, having N_T TA 74
elements, which are partitioned into M_T ABFs, each consisting of 75
 $U_T = N_T/M_T$ TA elements and the same number of analog phase 76

¹Note that in mmWave communications, the bandwidth expansion caused by
the SM-specific antenna switching [15] may not be a major problem, because a
wide bandwidth is available.

Manuscript received December 18, 2015; revised March 10, 2016; accepted
April 14, 2016. The work of N. Ishikawa was supported in part by the SCAT
Fellowship and in part by the MEXT/JASSO Tobitate Fellowship of Japan. The
work of S. Sugiura was supported by the Japan Society for the Promotion
of Science KAKENHI under Grant 26709028. The work of L. Hanzo was
supported by the European Research Council's Advanced Fellow Grant Beam-
Me-Up. The review of this paper was coordinated by Prof. Y. L. Guan.

N. Ishikawa and S. Sugiura are with the Department of Computer and
Information Sciences, Tokyo University of Agriculture and Technology, Tokyo
184-8588, Japan (e-mail: naoki@ishikawa.cc; sugiura@ieee.org).

R. Rajashekar and L. Hanzo are with the School of Electronics and Computer
Science, University of Southampton, Southampton SO17 1BJ, U.K. (e-mail:
R.Mysore-Rajashekar@soton.ac.uk; lh@ecs.soton.ac.uk).

Color versions of one or more of the figures in this paper are available online
at <http://ieeexplore.ieee.org>.

Digital Object Identifier 10.1109/TVT.2016.2555378

TABLE I
EXAMPLE OF THE GSM SYMBOLS FOR $(M_T, P) = (4, 2)$ AND $(8, 2)$

M_T	P	$\sqrt{P}\mathbf{x}$
4	2	$\begin{bmatrix} s_1 & s_2 & 0 & 0 \\ 0 & s_1 & 0 & s_2 \end{bmatrix}^T, \begin{bmatrix} s_1 & 0 & s_2 & 0 \\ 0 & 0 & s_1 & s_2 \end{bmatrix}^T,$
8	2	$\begin{bmatrix} s_1 & 0 & 0 & s_2 & 0 & 0 & 0 & 0 \\ s_1 & 0 & 0 & 0 & s_2 & 0 & 0 & 0 \\ s_1 & 0 & 0 & 0 & 0 & s_2 & 0 & 0 \\ s_1 & 0 & 0 & 0 & 0 & 0 & s_2 & 0 \\ 0 & s_1 & s_2 & 0 & 0 & 0 & 0 & 0 \\ 0 & s_1 & 0 & s_2 & 0 & 0 & 0 & 0 \\ 0 & s_1 & 0 & 0 & s_2 & 0 & 0 & 0 \\ 0 & s_1 & 0 & 0 & 0 & s_2 & 0 & 0 \end{bmatrix}^T, \begin{bmatrix} 0 & 0 & s_1 & s_2 & 0 & 0 & 0 & 0 \\ 0 & 0 & s_1 & 0 & 0 & s_2 & 0 & 0 \\ 0 & 0 & s_1 & 0 & 0 & 0 & s_2 & 0 \\ 0 & 0 & 0 & s_1 & 0 & s_2 & 0 & 0 \\ 0 & 0 & 0 & 0 & s_1 & 0 & s_2 & 0 \\ 0 & 0 & 0 & 0 & 0 & s_1 & 0 & s_2 \\ 0 & 0 & 0 & 0 & 0 & 0 & s_1 & 0 \\ 0 & 0 & 0 & 0 & 0 & 0 & 0 & s_1 \end{bmatrix}^T,$

77 shifters. In our GSM transmitter, the number of RF chains P is less 78 than the number of ABFs M_T , whereas the conventional spatial- 79 multiplexing scheme requires a full-RF structure having $P = M_T$.

80 At the GSM transmitter, B information bits are mapped into 81 a symbol vector $\mathbf{x} \in \mathbb{C}^{M_T \times 1}$ as follows. The B input bits are 82 serial-to-parallel converted into $B_1 = P \log_2(\mathcal{L})$ bits and $B_2 =$ 83 $\lceil \log_2 \binom{M_T}{P} \rceil$ bits. The B_1 bits are modulated to P complex-valued 84 symbols s_p ($p = 1, \dots, P$) with the aid of the classic quadrature 85 amplitude modulation (QAM) or phase-shift keying (PSK) scheme, 86 where the constellation size is given by \mathcal{L} . Based on the B_2 bits, 87 P out of M_T ABFs are activated, where P index vectors $\mathbf{a}_p \in$ 88 $\mathbb{C}^{M_T \times 1}$ ($p = 1, \dots, P$) are selected out of the M_T legitimate vectors 89 of $([1 \ 0 \ \dots \ 0]^T, [0 \ 1 \ \dots \ 0]^T, \dots, [0 \ 0 \ \dots \ 1]^T)$. Finally, the GSM 90 transmitter generates a symbol vector \mathbf{x} according to

$$\mathbf{x} = \frac{1}{\sqrt{P}} \sum_{p=1}^P s_p \mathbf{a}_p \quad (1)$$

91 which satisfies the average power constraint of $E[\|\mathbf{x}\|^2] = 1$, where 92 $E[\bullet]$ represents the expectation operation. In advance of trans- 93 missions, the symbol vector \mathbf{x} is precoded by a matrix $\mathbf{F} =$ 94 $\text{diag}(\mathbf{f}_1, \dots, \mathbf{f}_{M_T}) \in \mathbb{C}^{N_T \times M_T}$ [10], [11], where $\text{diag}(\bullet)$ represents 95 the block diagonalization, and $\mathbf{f}_i \in \mathbb{C}^{U_T \times 1}$ ($1 \leq i \leq M_T$) represents 96 the weight vectors of the i th ABF at the transmitter, which has the 97 constraint of $\|\mathbf{f}_i\|^2 = 1$.

98 To further elaborate, in Table I, we exemplify the GSM symbol sets 99 for the $(M_T, P) = (4, 2)$ and $(8, 2)$ scenarios. Furthermore, note that 100 the classic spatial multiplexing is a special case of the GSM scheme, 101 where the number of RF chains P is equal to the number of ABFs 102 M_T . Similarly, the conventional single-stream symbol transmission is 103 also subsumed by the GSM framework, where we have $P = 1$ and 104 $\mathbf{a}_1 = [1 \ 1 \ \dots \ 1]^T / \sqrt{M_T}$.

105 B. Channel Model

106 In this paper, we focus our attention on indoor mmWave commu- 107 nications, where a LoS component has the dominant effect [10]–[12], 108 [16], [17] in comparison to the non-LoS paths. More specifically, we 109 employ the frequency-flat Rician channel model. Fig. 2 shows the 110 alignment of the ABF-array transmitter and receiver. The spacing be- 111 tween the ABF arrays at the transmitter and the receiver is represented 112 by D_T and D_R , respectively. Moreover, d is the element separation of 113 each antenna element. The transmitter is located at a height of R . The 114 receiver has N_R antennas, and it is tilted at an angle of θ .

115 The Rician fading channels are given by [9], [10], [12]

$$\mathbf{H} = \sqrt{\frac{K}{K+1}} \mathbf{H}_{\text{LoS}} + \sqrt{\frac{1}{K+1}} \mathbf{H}_{\text{NLoS}} \in \mathbb{C}^{N_R \times N_T} \quad (2)$$

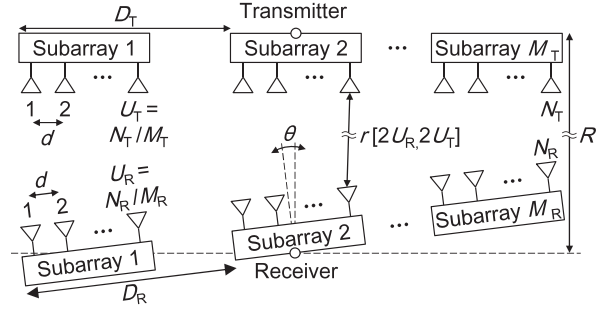


Fig. 2. ABF-array arrangement of our GSM transmitter and receiver. The transmitter is located at a height of R , and the receiver is tilted at an angle of θ .

where K is the Rice factor. Note that for the 60-GHz indoor communi- 116 cations scenario, the Rice factor K is in the range spanning from 8.34 117 to 12.04 dB [16]. Here, let us define the n th row and the m th column of 118 \mathbf{H}_{LoS} by $\mathbf{H}_{\text{LoS}}[n, m] = \exp(-j \cdot (2\pi/\lambda) \cdot r[n, m])$, where $r[n, m]$ 119 is the distance between the m th TA and the n th receive antenna, 120 whereas λ represents the wavelength. Furthermore, the n th row and the 121 m th column of \mathbf{H}_{NLoS} obeys the zero-mean complex-valued Gaussian 122 distribution, having a unit variance. 123

124 C. Receiver

Similar to the transmitter, the receiver consists of M_R ABFs, each 125 having $U_R = N_R/M_R$ antenna elements. The receiver is equipped 126 with the same number of RF chains as that of the ABFs, hence having 127 a full-RF structure of $P = M_R$. The signals received at the M_R ABFs 128 are given by 129

$$\mathbf{y} = \underbrace{\mathbf{W}^H \mathbf{H} \mathbf{F}}_{\mathbf{H}_b} \mathbf{x} + \mathbf{n} \in \mathbb{C}^{M_R} \quad (3)$$

where $\mathbf{W} = \text{diag}(\mathbf{w}_1, \dots, \mathbf{w}_{M_R}) \in \mathbb{C}^{N_R \times M_R}$ [10], [11] is the ABF 130 weight matrix associated with the analog phase shifters at the re- 131 ceiver, which satisfies the constraint of $\|\mathbf{w}_k\|^2 = 1$ ($1 \leq k \leq M_R$). 132 Furthermore, $\mathbf{n} \in \mathbb{C}^{M_R \times 1}$ denotes the additive white Gaussian noise 133 having the variance of N_0 , whereas $\mathbf{W}^H \mathbf{H} \mathbf{F}$ is represented by the 134 equivalent channel matrix $\mathbf{H}_b \in \mathbb{C}^{M_R \times M_T}$. In this paper, we assume 135 that the receiver acquires accurate channels \mathbf{H}_b with the aid of pilot 136 symbols transmitted from the transmitter. Furthermore, the direction 137 between the transmitter and the receiver is also known, which is used 138 to determine the ABF weights \mathbf{F} and \mathbf{W} at the transmitter and the 139 receiver, as will be shown in Section III-D. 140

Finally, the receiver estimates the transmitted information bits 141 (B_1, B_2) , based on the maximum-likelihood criterion as follows: 142

$$(\hat{B}_1, \hat{B}_2) = \arg \min_{(B_1, B_2)} \|\mathbf{y} - \mathbf{H}_b \mathbf{x}\|^2. \quad (4)$$

The reduced-complexity detection algorithms [2], [3], [18] developed 143 for the GSM are readily applicable to the proposed receiver. 144

145 III. CHANNEL CAPACITY

Here, we review the continuous-input–continuous-output memo- 146 ryless channel (CCMC) capacity and the discrete-input–continuous- 147 output memoryless channel (DCMC) capacity for our mmWave GSM 148 scheme. The CCMC capacity is derived by assuming that the input 149 signal obeys the Gaussian distribution, whereas in the derivation of the 150 DCMC capacity, a specific finite-alphabet input symbol set is assumed. 151

152 A. CCMC Capacity

153 The classic CCMC capacity C_{CCMC} is given by [10], [14]

$$C_{\text{CCMC}} = E_{\mathbf{H}} \left[\sum_{i=1}^{\text{rank}(\mathbf{Q})} \log_2(1 + \mu_i \rho) \right] \text{ [bits/symbol]} \quad (5)$$

154 where we have

$$\mathbf{Q} = \begin{cases} \mathbf{H}_b^H \mathbf{H}_b & (M_R \geq M_T) \\ \mathbf{H}_b \mathbf{H}_b^H & (M_R < M_T). \end{cases} \quad (6)$$

155 Here, μ_i is the i th eigenvalue of the Hermitian matrix \mathbf{Q} , while
 156 assuming continuous-amplitude discrete-time signaling. Moreover, ρ
 157 represents the signal-to-noise ratio (SNR). In the CCMC capacity of
 158 (5), the employment of ideal ABF weights \mathbf{F} and \mathbf{W} is assumed at the
 159 transmitter and the receiver, where \mathbf{F} is the M_T right singular vectors
 160 of \mathbf{H} associated with the maximum singular values. Similarly, \mathbf{W} is
 161 the M_R left singular vectors of \mathbf{H} .

162 B. DCMC Capacity

163 Let us now introduce the DCMC capacity C_{DCMC} of mmWave
 164 MIMO systems as follows [19], [20]:

$$C_{\text{DCMC}} = B - \frac{1}{2^B} \sum_{f=1}^{2^B} E_{\mathbf{H}, \mathbf{n}} \left[\log_2 \sum_{g=1}^{2^B} e^{\eta[f, g]} \right] \text{ [bits/symbol]} \quad (7)$$

165 where we have

$$\eta[f, g] = \frac{-\|\mathbf{H}_b(\mathbf{x}_f - \mathbf{x}_g) + \mathbf{n}\|^2 + \|\mathbf{n}\|^2}{N_0} \quad (8)$$

166 and \mathbf{x}_i ($i = 1, \dots, 2^B$) represents the legitimate symbol vectors.
 167 The ABF weight matrices \mathbf{F} and \mathbf{W} are generated according to the
 168 criteria presented in Section III-D. Note that powerful channel coding
 169 schemes, such as the turbo codes or low-density parity-check codes,
 170 allow us to attain a near-error-free performance close to the DCMC
 171 capacity [21].

172 C. Optimization of ABF-Array Alignment

173 As previously mentioned, the rank of the MIMO channel matrix
 174 in an indoor mmWave scenario is typically low. To circumvent this
 175 problem, we optimize the ABF-array alignment according to [9],
 176 which increases the rank of the channel matrix. More specifically, to
 177 attain the optimum performance in terms of the rank of the channel
 178 matrix, the separations of the ABFs D_T and D_R at the transmitter and
 179 the receiver have to satisfy the following relationship [9]–[11]:

$$D_T D_R = \frac{\lambda R}{\max(M_T, M_R) \cos(\theta)} \quad (9)$$

180 where the maximum rank of the channel matrix is given by
 181 $\text{rank}(\mathbf{H}_b) = \min(M_T, M_R)$.

182 D. Criterion for Determining the ABF Weights

183 If the transmitter knows the accurate estimates of the channel \mathbf{H} ,
 184 which has as many as $(N_T \cdot N_R)$ channel coefficients, it is possible
 185 to carry out optimum beamforming at the transmitter and the receiver.
 186 However, in practice, it may be a challenging task to acquire all the
 187 $(N_T \cdot N_R)$ channel coefficients, particularly for a large-scale MIMO
 188 scenario. Hence, in this paper, we control the ABFs based only on
 189 the angle-of-departure (AoD) θ_{AoD} and the angle-of-arrival (AoA)

TABLE II
SYSTEM PARAMETERS

Fig.	Rate	Scheme	RF	\mathcal{L}	Rate	Scheme	RF	\mathcal{L}
3	4.0	BF	1	16	8.0	BF	1	256
	4.0	BLAST	2	4	8.0	BLAST	2	16
	4.0	BLAST	4	2	8.0	BLAST	4	4
	4.0	GSM	1	4	8.0	GSM	1	64
	4.0	GSM	2	2	8.0	GSM	2	8
4	8.0	BF	1	256	16.0	BF	1	65536
	8.0	BLAST	2	16	16.0	BLAST	2	256
	8.0	BLAST	8	2	16.0	BLAST	8	4
	8.0	GSM	1	32	17.0	GSM	1	16384
	8.0	GSM	2	4	16.0	GSM	2	64

θ_{AoA} at the transmitter and the receiver, respectively. This significantly
 190 reduces the number of channel coefficients that have to be estimated
 191 from the transmitted pilot symbols, namely, from $(N_T \cdot N_R)$ to $(M_T \cdot 192$
 $M_R)$, which is lower than that needed for the full-digital array. More
 193 specifically, the ABF weights \mathbf{f}_i and \mathbf{w}_k are given by [10], [13] 194

$$\mathbf{f}_i = \frac{1}{\sqrt{U_T}} \left[1, \exp(j\delta_T^{(i)}), \dots, \exp(j(U_T - 1)\delta_T^{(i)}) \right]^T$$

$$\mathbf{w}_k = \frac{1}{\sqrt{U_R}} \left[1, \exp(j\delta_R^{(k)}), \dots, \exp(j(U_R - 1)\delta_R^{(k)}) \right]^T$$

where we have $\delta_T^{(i)} = d \cdot (2\pi/\lambda) \cdot \sin(\theta_{\text{AoD}}^{(i)})$ and $\delta_R^{(k)} = d \cdot (2\pi/\lambda) \cdot 195$
 $\sin(\theta_{\text{AoA}}^{(k)})$.² Here, $\theta_{\text{AoD}}^{(i)}$ denotes the AoD toward the i th ABF of the 196
 receiver, whereas $\theta_{\text{AoA}}^{(k)}$ represents the AoA from the k th ABF of the 197
 transmitter. 198

IV. PERFORMANCE RESULTS

199

Here, we provide our performance results to characterize the ca-
 200 pacity of our GSM scheme, which is compared with the single-stream
 201 BF and the spatial-multiplexing benchmark schemes. Throughout the
 202 simulations, we assumed the indoor mmWave scenario in Fig. 2,
 203 where we have an antenna height of $R = 5$ m. We considered the
 204 carrier frequency of 60 GHz, where the corresponding wavelength was
 205 $\lambda = 0.5$ cm. The Rice factor K was set to 10.0 dB in accordance with
 206 the work in [11]. The antenna spacing d in each ABF was fixed to $\lambda/2$,
 207 and the separation between ABFs was optimized based on (9). The
 208 employment of omnidirectional antenna elements was assumed both
 209 at the transmitter and the receiver. Furthermore, system parameters of
 210 all schemes are listed in Table II. 211

Fig. 3 compares the DCMC capacity of the GSM, the spatial-
 212 multiplexing, and the single-stream BF schemes, where the data rates
 213 were 4.0 bits/symbol (top) and 8.0 bits/symbol (bottom). The transmit-
 214 ter and the receiver have $N_T = N_R = 16$ antenna elements, which are
 215 grouped into $M_T = M_R = 4$ ABFs, where the separation of ABFs
 216 was $D_T = D_R = 7.91$ cm. In this scenario, the rank of the chan-
 217 nel matrix was $\text{rank}(\mathbf{H}_b) = \min(4, 4) = 4$. For the 4.0-bits/symbol
 218 scenario, we considered the 16-QAM single-input single-output (SISO)
 219 scheme, the binary phase-shift keying (BPSK)-aided spatial multi-
 220 plexing having $P = 4$ RF chains, the quaternary phase-shift keying
 221 (QPSK)-aided single-RF GSM scheme, and the BPSK-aided GSM
 222 having $P = 2$ RF chains. Additionally, the capacity curve of the
 223 QPSK-aided spatial-multiplexing scheme using $P = 2$ RF chains
 224 was plotted. For the case of 8.0 bits/symbol, the 256-QAM SISO
 225 scheme, the QPSK-aided spatial-multiplexing scheme having $P = 4$
 226 RF chains, the 16-QAM-aided spatial-multiplexing scheme using 227

²Potentially, the channel state information available at the transmitter allows
 us to utilize the phase-rotation-based precoding scheme in [22].

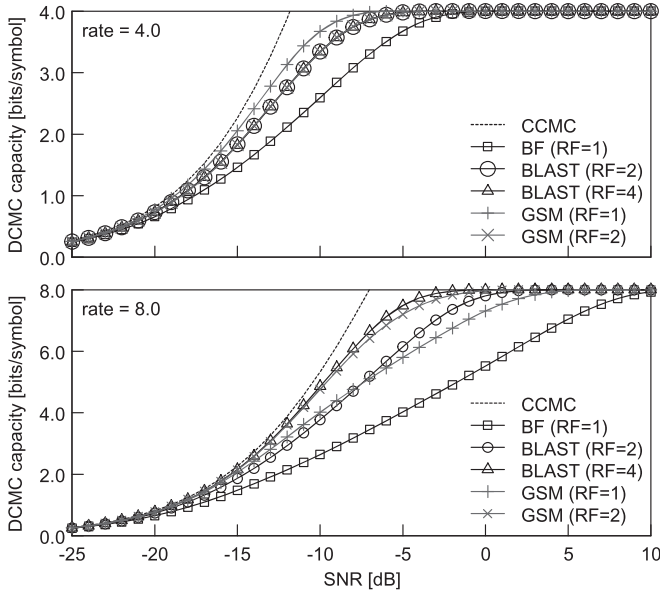


Fig. 3. DCMC capacity comparisons between the GSM and other benchmarks. The transmitter and the receiver had four ABFs, each having four antenna elements and four analog phase shifters. The associated CCMC capacity was also plotted.

228 $P = 2$ RF chains, the 64-QAM single-RF GSM scheme, and the
 229 8-PSK GSM scheme having $P = 2$ RF chains were considered. Observe
 230 in Fig. 3 that for the rate of 4.0 bits/symbol, the single-RF GSM outper-
 231 formed the other schemes. Moreover, the DCMC capacity of the GSM
 232 having $P = 2$ RF chains was close to those of the spatial-multiplexing
 233 schemes that employ $P = 2$ and 4 RF chains. Furthermore, for the rate
 234 of 8.0 bits/symbol, the DCMC capacity of the single-RF GSM scheme
 235 achieved comparable performance to that of the spatial-multiplexing
 236 scheme having $P = 2$ RF chains, whereas the DCMC capacity of the
 237 GSM scheme having $P = 2$ RF chains and the spatial-multiplexing
 238 scheme having $P = 4$ RF chains exhibited a similar performance at
 239 the transmission rate of 4.0 bits/symbol. According to our extensive
 240 simulations, it was found that the performance advantage of the
 241 proposed scheme remains unchanged in the range of $1 \leq R \leq 5$ m.

242 Moreover, Fig. 4 shows the DCMC capacity of the GSM, of the
 243 BLAST, and of the SISO schemes for the data rates of 8.0 bits/symbol
 244 (top) and 16.0 bits/symbol (bottom). The transmitter and the receiver
 245 have $N_T = 32$ and $N_R = 16$ antenna elements, respectively, where
 246 the transmitter has $M_T = 8$ ABFs, and the receiver has $M_R = 4$ ABFs.
 247 Here, the optimized separation between ABFs was $D_T = D_R =$
 248 5.59 cm. In this scenario, the rank of the channel matrix was
 249 $\text{rank}(\mathbf{H}_b) = \min(8, 4) = 4$. For the rate of 8.0 bits/symbol, the
 250 256-QAM SISO scheme, the BPSK-aided spatial-multiplexing scheme
 251 having $P = 8$ RF chains, the 16-QAM spatial-multiplexing scheme
 252 using $P = 2$ RF chains, the 32-PSK single-RF GSM scheme, and
 253 the QPSK-aided GSM using $P = 2$ RF chains were considered. For
 254 the case of 16.0 bits/symbol, the 65536-QAM SISO scheme, the
 255 QPSK-aided spatial-multiplexing scheme having $P = 8$ RF chains,
 256 the 256-QAM spatial-multiplexing scheme having $P = 2$ RF chains,
 257 the 16384-QAM single-RF GSM scheme, and the 64-QAM GSM
 258 scheme having $P = 2$ RF chains were compared. For ease of compari-
 259 son, the data rate of the single-RF GSM was set to 17.0 bits/symbol. It
 260 was shown in Fig. 4 that for the rate of 8.0 bits/symbol, the DCMC ca-
 261 pacity of the GSM scheme having two RF chains was the highest. For
 262 the rate of 16.0 bits/symbol, the full-RF spatial-multiplexing scheme
 263 exhibited the best capacity over the entire SNR region, whereas the
 264 GSM scheme having two RF chains achieved capacity close to that of

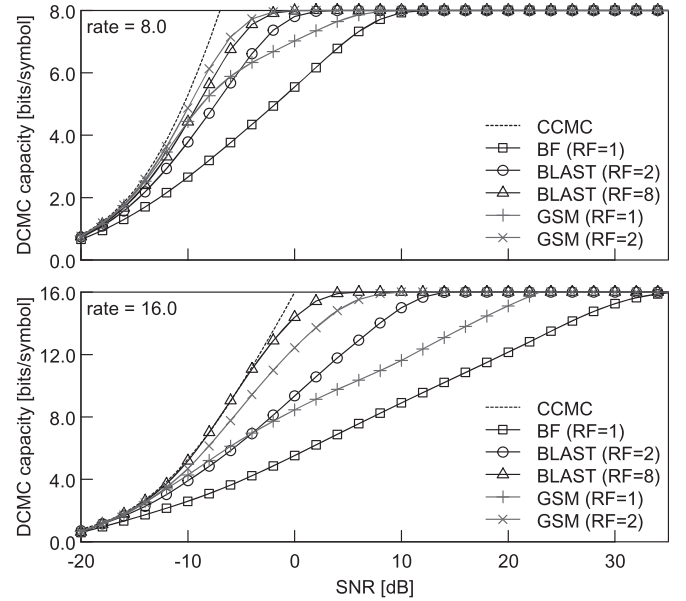


Fig. 4. DCMC capacity comparisons between the GSM and other benchmarks. The transmitter consists of eight ABFs, each having four TA elements, whereas the receiver has four ABFs, each having four receive antenna elements. The associated CCMC capacity was also plotted.

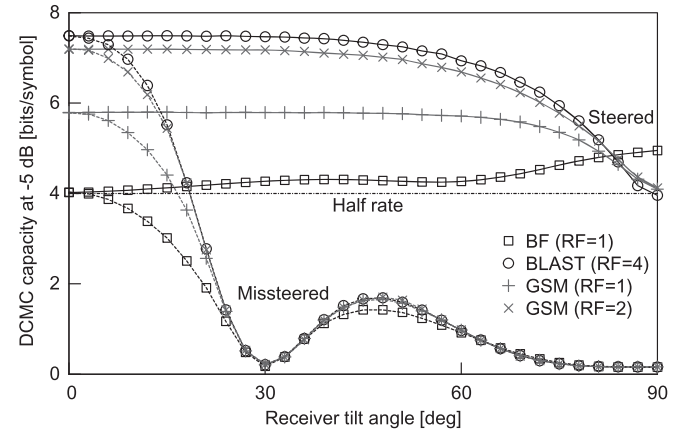


Fig. 5. Effects of the estimated tilt angle $\hat{\theta}$ on the DCMC capacity at the SNR of -5 dB. The system parameters were the same as those used in Fig. 3.

the full-RF spatial-multiplexing scheme, where the performance gap
 265 was as low as 1.2 dB for the DCMC capacity of 8.0 bits/symbol. Note
 266 that the performance advantage of the single-RF GSM scheme was
 267 approximately 9.0 dB.
 268

Finally, in Fig. 5, we investigated the effects of the receiver tilt θ ,
 269 where the system parameters were the same as those used in Fig. 3
 270 (8.0 bits/symbol). The DCMC capacity was calculated at the SNR
 271 of -5 dB. We also considered the missteered scenario, where the
 272 estimated θ_{AoD} and θ_{AoA} were fixed to 0° . The three capacity curves
 273 of the missteered scenario exhibited two peaks, namely, at $\theta = 0^\circ$ and
 274 45° , which corresponded to the directive gains of the main lobe and
 275 the sidelobe. When θ_{AoD} and θ_{AoA} were accurately estimated, the
 276 capacity of the GSM and of the spatial-multiplexing schemes remained
 277 high for the range of $0 \leq \theta < 83^\circ$.
 278

V. CONCLUSION

279

In this paper, we have proposed a GSM-based reduced-RF-chain
 280 mmWave MIMO system, where the transmitter consists of ABF arrays. 281

282 In our simulations, we demonstrated that the constrained capacity of
 283 our GSM scheme was close to that of its full-RF spatial-multiplexing
 284 counterpart, which is equipped with twice or four times higher number
 285 of RF chains than the proposed GSM scheme.

REFERENCES

- 286
 287 [1] R. Y. Mesleh, H. Haas, S. Sinanovic, C. Ahn, and S. Yun, "Spatial
 288 modulation," *IEEE Trans. Veh. Technol.*, vol. 57, no. 4, pp. 2228–2241,
 289 Jul. 2008.
- 290 [2] S. Sugiura, C. Xu, S. Ng, and L. Hanzo, "Reduced-complexity coherent
 291 versus non-coherent QAM-aided space–time shift keying," *IEEE Trans.*
 292 *Commun.*, vol. 59, no. 11, pp. 3090–3101, Nov. 2011.
- 293 [3] C. Xu, S. Sugiura, S. X. Ng, and L. Hanzo, "Spatial modulation
 294 and space–time shift keying: Optimal performance at a reduced detec-
 295 tion complexity," *IEEE Trans. Commun.*, vol. 61, no. 1, pp. 206–216,
 296 Jan. 2013.
- 297 [4] M. Di Renzo, H. Haas, A. Ghayeb, S. Sugiura, and L. Hanzo, "Spatial
 298 modulation for generalized MIMO: Challenges, opportunities, and imple-
 299 mentation," *Proc. IEEE*, vol. 102, no. 1, pp. 56–103, Jan. 2014.
- 300 [5] J. Jeganathan, A. Ghayeb, and L. Szczecinski, "Generalized space shift
 301 keying modulation for MIMO channels," in *Proc. IEEE Int. Symp.*
 302 *PIMRC*, Sep. 2008, pp. 1–5.
- 303 [6] S. Sugiura, S. Chen, and L. Hanzo, "Generalized space–time shift
 304 keying designed for flexible diversity-, multiplexing- and complexity-
 305 tradeoffs," *IEEE Trans. Wireless Commun.*, vol. 10, no. 4, pp. 1144–1153,
 306 Apr. 2011.
- 307 [7] P. Wolniansky, G. Foschini, G. Golden, and R. Valenzuela, "V-BLAST:
 308 An architecture for realizing very high data rates over the rich-scattering
 309 wireless channel," in *Proc. ISSSE*, 1998, pp. 295–300.
- 310 [8] S. Rangan, T. S. Rappaport, and E. Erkip, "Millimeter-wave cellular wire-
 311 less networks: Potentials and challenges," *Proc. IEEE*, vol. 102, no. 3,
 312 pp. 366–385, Mar. 2014.
- 313 [9] F. Bøhagen, P. Orten, and G. E. Øien, "Design of optimal high-rank line-
 314 of-sight MIMO channels," *IEEE Trans. Wireless Commun.*, vol. 6, no. 4,
 315 pp. 1420–1424, Apr. 2007.
- [10] E. Torkildson, U. Madhoo, and M. Rodwell, "Indoor millimeter wave 316
 MIMO: Feasibility and performance," *IEEE Trans. Wireless Commun.*, 317
 vol. 10, no. 12, pp. 4150–4160, Dec. 2011. 318
- [11] L. Zhou and Y. Ohashi, "Fast codebook-based beamforming training for 319
 mmWave MIMO systems with subarray structures," in *Proc. IEEE 82nd* 320
Veh. Technol. Conf., 2015, pp. 1–5. 321
- [12] P. Liu and A. Springer, "Space shift keying for LOS communication 322
 at mmWave frequencies," *IEEE Wireless Commun. Lett.*, vol. 4, no. 2, 323
 pp. 121–124, Apr. 2015. 324
- [13] Y. J. Guo, X. Huang, and V. Dyadyuk, "A hybrid adaptive antenna ar- 325
 ray for long-range mm-wave communications," *IEEE Antennas Propag.* 326
Mag., vol. 54, no. 2, pp. 271–282, Apr. 2012. 327
- [14] O. E. Ayach, S. Rajagopal, S. Abu-Surra, Z. Pi, and R. W. Heath, "Spa- 328
 tially sparse precoding in millimeter wave MIMO systems," *IEEE Trans.* 329
Wireless Commun., vol. 13, no. 3, pp. 1499–1513, Mar. 2014. 330
- [15] K. Ishibashi and S. Sugiura, "Effects of antenna switching on band- 331
 limited spatial modulation," *IEEE Wireless Commun. Lett.*, vol. 3, no. 4, 332
 pp. 345–348, Aug. 2014. 333
- [16] I. Sarris and A. R. Nix, "Rician K-factor measurements in a home and 334
 an office environment in the 60 GHz band," in *Proc. 16th IST Mobile* 335
Wireless Commun. Summit, 2007, pp. 1–5. 336
- [17] Y. Shoji, H. Sawada, C. S. Choi, and H. Ogawa, "A modified SV-model 337
 suitable for line-of-sight desktop usage of millimeter-wave WPAN sys- 338
 tems," *IEEE Trans. Antennas Propag.*, vol. 57, no. 10, pp. 2940–2948, 339
 Oct. 2009. 340
- [18] R. Rajashekar, K. V. S. Hari, and L. Hanzo, "Reduced-complexity ML de- 341
 tection and capacity-optimized training for spatial modulation systems," 342
IEEE Trans. Commun., vol. 62, no. 1, pp. 112–125, Jan. 2014. 343
- [19] S. X. Ng and L. Hanzo, "On the MIMO channel capacity of multi- 344
 dimensional signal sets," *IEEE Trans. Veh. Technol.*, vol. 55, no. 2, 345
 pp. 528–536, Mar. 2006. 346
- [20] S. Sugiura, S. Chen, and L. Hanzo, "Coherent and differential space–time 347
 shift keying: A dispersion matrix approach," *IEEE Trans. Commun.*, 348
 vol. 58, no. 11, pp. 3219–3230, Nov. 2010. 349
- [21] L. Hanzo, O. Alamri, M. El-Hajjar, and N. Wu, *Near-Capacity Multi-* 350
Functional MIMO Systems. New York, NY, USA: Wiley, 2009. 351
- [22] P. Yang *et al.*, "Phase rotation-based precoding for spatial modulation 352
 systems," *IET Commun.*, vol. 9, no. 10, pp. 1315–1323, Jul. 2015. 353

AUTHOR QUERY

NO QUERY.